GeoScienceWorld
Lithosphere
Volume 2022, Article ID 6913641, 21 pages
https://doi.org/10.2113/2022/6913641

Lithosphere

Research Article

Reservoir Modeling of Braided River Reservoirs Based on Geological Knowledge Database: A Case Study of P_1x Formation of the Daniudi Gas Field, Ordos Basin, China

Mengjiao Dou,[1] **Shaohua Li**,[1] **Tao Lei**,[2] **Guanglei Ren**,[2] **Xiaohui Li**,[2] **Ying Guo**,[2] **and Wenjie Feng**[1]

[1]*School of Geosciences, Yangtze University, Wuhan 430100, China*
[2]*Exploration and Development Institute, Huabei Branch Company of Sinopec, Zhengzhou 450006, China*

Correspondence should be addressed to Shaohua Li; lish@yangtzeu.edu.cn

Received 3 May 2022; Revised 12 September 2022; Accepted 14 September 2022; Published 13 October 2022

Academic Editor: Qian Liu

The sandy braided river depositional system developed in the Lower Shihezi Formation of the Daniudi gas field, Ordos Basin. It has the characteristics of frequent migration and oscillation of braided channels and large well spacing, making it challenging to portray the braided river sand body in this area, bringing uncertainty to the 3D geological modeling of the reservoir. This study takes the primary gas reservoir H1 member as an example. It establishes a quantitative geological knowledge database for the reservoir by statistically fitting the correlation equations between the braided channel and channel bar in the planes and profiles to reduce the uncertainty of reservoir modeling. This study combines the multisource and multiscale information from modern sedimentation, field outcrops, and tank simulation experiments of the braided river. From the data, the distribution intervals for the thickness and width of the braided channel sand body in the H1 member are 1–22 m and 7–320 m, respectively, and the thickness, width, and length distribution intervals of the sand body in the channel bar are 3–30 m, 80–1500 m, and 240–4200 m, respectively. A 3D training image is established using the object-based simulation method based on the H1 member's well data and combining the quantitative parameters of various microfacies in the geological knowledge database. The multiple-point geostatistical modeling method is applied to establish a sedimentary microfacies model. The model's uncertainty is reduced through multi-information fusion constraint modeling, providing a reliable basis for guiding the prediction of the remaining gas in the Daniudi gas field.

1. Introduction

Establishing and expanding quantitative geological knowledge databases for several reservoirs have attracted considerable attention in recent decades [1–6]. Several strategies have been used in studies on establishing geological knowledge databases via quantitative geology, such as the fine anatomy of reservoirs in dense well network development areas [7, 8], field outcrop anatomy [9–11], modern sedimentation anatomy [12], tank simulation experiments [13], 3D digital outcrop model [14–16], 3D seismic data analysis [3, 17], Google Earth satellite image analysis [18–21], and remote sensing image analysis [22]. Several studies have focused on the geological information database of braided river reservoirs in the Ordos Basin, for example, Zhang et al. [8], Shi et al. [7], and Xu et al. [19] for the Sulige gas field reservoir and Zhang et al. [23] for the Hangjinqi area, combined modern sedimentation based on Google Earth measurements, outcrop data, and dense well network anatomy to establish a quantitative geological knowledge database of braided river reservoirs. They established a microfacies model using the multiple-point geostatistical modeling method based on 3D training images of quantitative characterization and received rich

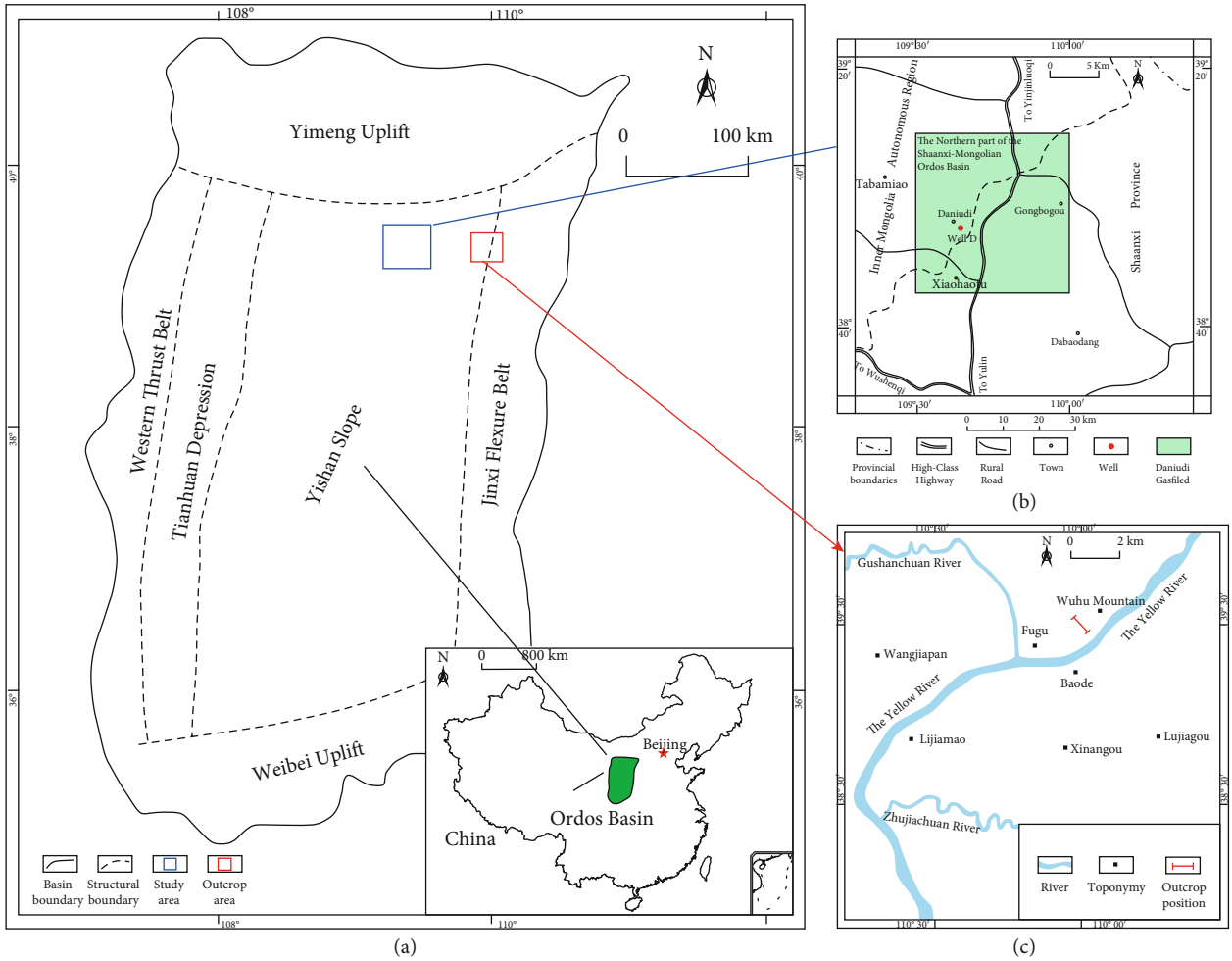

Figure 1: Location of the study area. (a) The location of the Ordos Basin (after Xu et al. [33]). (b) The location of the Daniudi Gas field (after Wu. [31]). (c) The location of the Fugu Tianshengqiao in the field outcrop (after Chen [32]).

results. However, most are limited to using traditional geological dissection methods in the process, and the geological knowledge databases associated with the Daniudi gas field have received less attention in previous research.

A sandy braided river is a vital terrestrial sedimentary system. However, due to its reservoir's substantial heterogeneity, the sand body's spatial stacking pattern and distribution are complex, making it challenging to establish a highly reliable 3D geological model of the braided river reservoir [24]. Academics have extensively studied modeling braided river reservoirs. Li et al. [25] used a plane facies-controlled method to establish a 3D geological model of the braided river, analyzed the development pattern of nonpermeable layers inside the reservoir, and predicted the distribution of interbeds. Ma et al. [26] integrated dynamic and static information to demonstrate the scale of different sand body levels through sand connectivity analysis to establish a 3D geological model. Chen et al. [27] restricted the braided river reservoir geological model by collecting genetic and evolution information from well and seismic data and identifying genetic unit types and features. Wu et al. [28] established a spatial spreading model of a braided river reservoir consistent with architectural knowledge by identifying and predicting the constitutive unit's scale and using a hierarchically restricted embedded modeling technique.

In the Lower Shihezi Formation of the Daniudi gas field in Ordos Basin, it develops a braided river sedimentary system, making it challenging to portray this area's braided river sand body and bringing uncertainty to the reservoir's 3D geological modeling because of its frequent migration and oscillation of braided channels and its large well spacing. Therefore, we integrate multisource and multiscale information from similar modern deposits, digital outcrop profiles in the field, and tank simulation experiments to establish a quantitative geological knowledge database for the braided river reservoir in the Lower Shihezi Formation H1 member of the Daniudi gas field. We rely on multiscale data to synthesize the empirical formulas for the scale of various microfacies units and on subsurface well data from the research area to compare the present with the past. The object-based method is employed to establish a 3D training image that conforms to the study area's geological characteristics

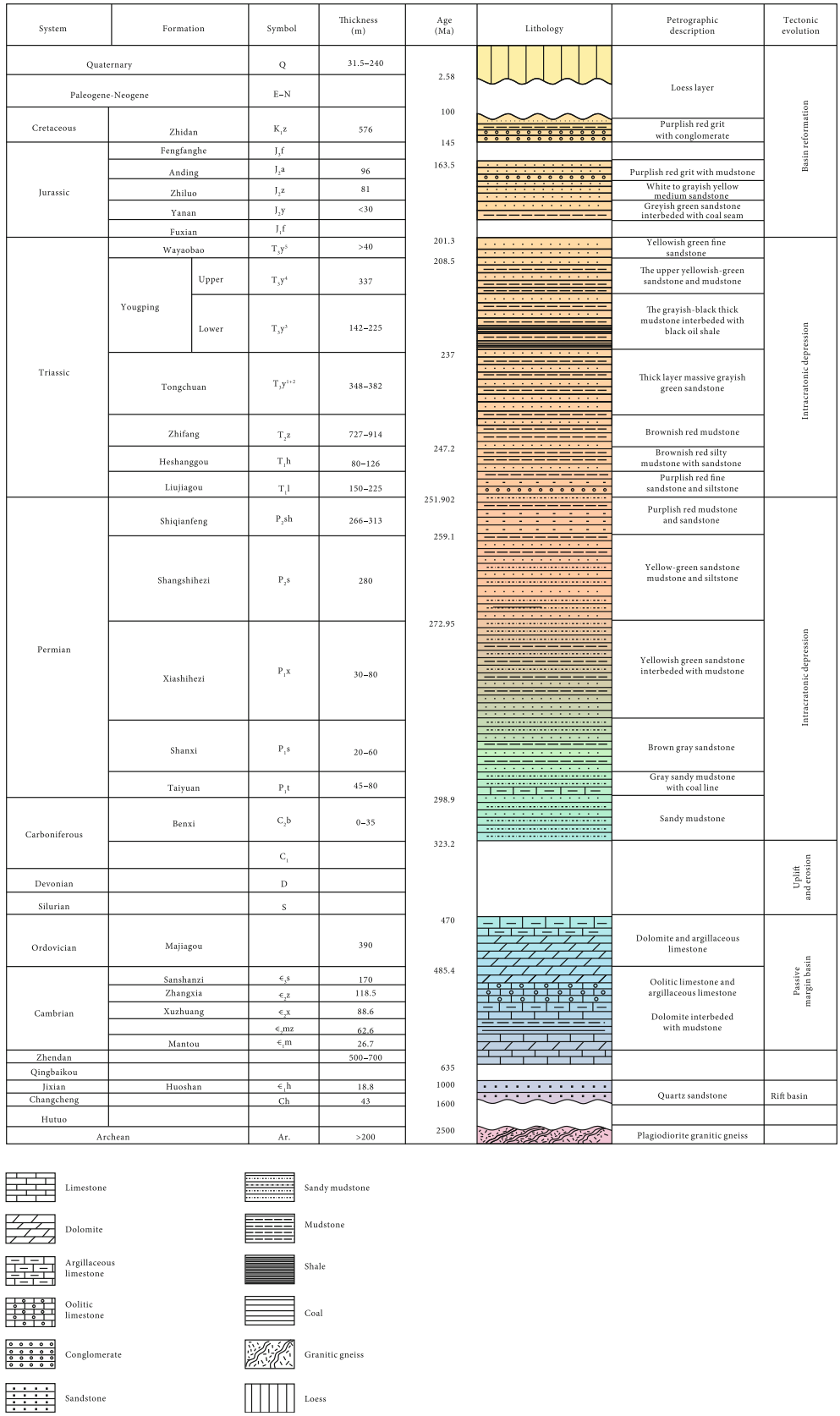

Figure 2: Stratigraphic column of the Shihezi Formation in the study area (modified from Xu and He [35]).

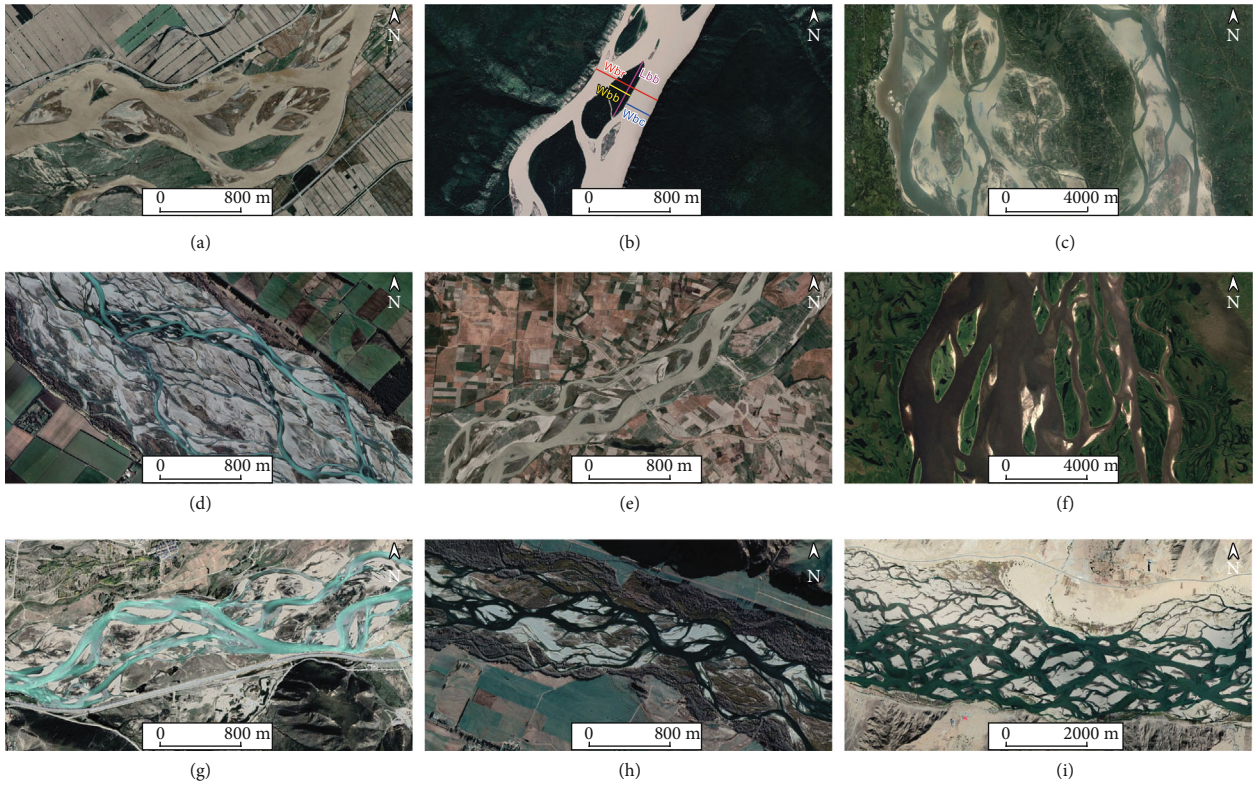

FIGURE 3: Distribution characteristics of modern sandy braided river channel bars and active braided channels. (a) Yellow River, (b) Yukon River, (c) Jamuna River, (d) Rakaia River, (e) Ganges River, (f) Lena River, (g) Lhasa River, (h) Waitaki River, and (i) Brahmaputra River. Wbb: width of braided bar; Lbb: length of braided bar; Wbc: width of braided channel; Wbr: width of braided river.

based on the knowledge database of quantitative parameters. Furthermore, the multiple-point geostatistical modeling method is applied to establish a sedimentary facies model that conforms to geological understanding laws and deposition patterns, reducing model uncertainty and laying a solid foundation for forecasting the remaining gas in the Daniudi gas field.

2. Geological Setting

The Ordos Basin is in North-Central China (Figure 1(a)). The Ordos Basin is a large multirotational craton-margin stacked basin with depressional migration, subsidence, and tectonic simplicity [29]. It is divided into six primary tectonic units: the Yimeng Uplift to the north, the Weibei Uplift to the south, the Western Thrust Belt and the Tianhuan Depression to the west, the Jinxi Flexural Belt to the east, and the Yishaan Slope in the center [30]. The Daniudi gas field's regional tectonics is in the northeastern part of the Yishaan Slope, a secondary tectonic unit of the basin [31] (Figure 1(b)). The surrounding sedimentary outcrop is approximately 130 km east of the Daniudi gas field and tectonically to the north of the Jinxi Flexural Belt in the basin [32] (Figure 1(c)). Regarding the target reservoir, depositional environment, and reservoir features, the Fugu Tianshengqiao profile is comparable to the Daniudi gas field. The section's primary body is northeast-southwest trending, with good overall outcrop conditions that are easy to observe, describe, and sample for analysis.

The Permian Lower Shihezi Formation is divided into three members from the bottom to the top: H1 (P_1x^1), H2 (P_1x^2), and H3 (P_1x^3). H1 is the primary gas-bearing section with undeveloped fractures in the target layer and gentle tectonics—a gentle high northeast and low southwest monocline [31, 34]. The local development of a nose uplift with a near east–west trend does not constitute a larger tectonic enclosure. The Shihezi Formation of the Daniudi gas field has braided river deposits with a floodplain and braided river subfacies. In the braided river system, the braided channel subfacies are the primary facies of sandstone deposition, with two microfacies evolved, namely, the channel bar and the braided channel between the channel bars (Figure 2). Sand conglomerate, pebbly sandstone, fine sandstone, siltstone, and mudstone dominate the lithology, and the burial thickness is 2540–2840 m.

3. Databases and Methods

This study focuses on the H1 member of the Shihezi Formation in the Daniudi gas field, one of the most gas-rich areas. Currently, approximately 296 wells have been drilled, covering approximately 188 km^2. The density is 0.635 km^2/well,

Table 1: Statistics of modern sedimentary channel bar and braided channel scale parameters.

Braided river name	Case	Width of braided bar (m)	Length of braided bar (m)	Width of channel (m)	Width of braided river (m)	Braided river name	Case	Width of braided bar (m)	Length of braided bar (m)	Width of channel (m)	Width of braided river (m)
Yellow River	1	227.54	789.66	123.38	1704.76	Ganges River	6	47.6	119.36	93.7	384.89
Yellow River	2	185.46	493.39	66.65	952.42	Ganges River	7	178.03	442.2	45.87	681.13
Yellow River	3	188.13	353.15	21.78	1317.75	Ganges River	8	83.14	205.47	113.8	535.67
Yellow River	4	78.23	240.13	51.56	873.98	Ganges River	9	62.5	341.09	112.11	619.1
Yellow River	5	143.1	405.75	112.4	883.35	Ganges River	10	212.19	461.08	79.04	308.94
Yellow River	6	114.43	386.03	59.62	834.21	Lena River	1	1361.15	3995.3	524.96	15250.7
Yellow River	7	172.55	635.52	51.22	1298.39	Lena River	2	1879.18	6642.29	567.15	10791.67
Yellow River	8	56.34	196.19	50.54	700.18	Lena River	3	2373.88	8625.46	862.38	14431.71
Yellow River	9	156.52	363.03	47.55	938.89	Lena River	4	4408.26	11214.2	848.69	14493.79
Yellow River	10	51.64	147.93	46.01	1113	Lena River	5	2172.01	5603.23	732.03	12477.07
Yukon River	1	278.77	978.78	246.58	1033.68	Lena River	6	3257.02	10123.24	962.84	13541.14
Yukon River	2	201.95	443.66	33.19	1461.93	Lena River	7	1476.51	6159.28	209.25	10193.61
Yukon River	3	266.55	676.94	53.32	1272.59	Lena River	8	4287.4	10107.75	980.42	12131.56
Yukon River	4	169.37	578.73	85.91	1154.39	Lena River	9	1604.16	5460.48	594.49	10563.79
Yukon River	5	252.9	663.71	106.46	1062.44	Lena River	10	2774.31	11053.23	911.24	9704.57
Yukon River	6	436.77	1651.73	161.94	1424.44	Lhasa River	1	128.74	408.6	38.82	521.11
Yukon River	7	514.19	1493.49	90.43	1068.22	Lhasa River	2	112.31	428.69	33.54	1783.11
Yukon River	8	187.57	521.44	84.32	1899.59	Lhasa River	3	371.73	930.03	27.56	1866.36
Yukon River	9	170.21	585.92	30.81	1572.4	Lhasa River	4	229.27	477.15	53.6	738.18
Yukon River	10	221.28	683.75	36.38	1768.34	Lhasa River	5	234.25	647.15	53.5	721.65
Jamuna River	1	1398.79	4183.5	468.8	16114.11	Lhasa River	6	97.39	533.03	48.18	592.75
Jamuna River	2	2262.82	6759.15	1026.99	8675.27	Lhasa River	7	75.82	236.8	44.19	609.49
Jamuna River	3	1859.83	3673.94	808.44	9973.46	Lhasa River	8	268.13	905.17	70.99	864.72
Jamuna River	4	975.34	3561.61	611.86	12429.61	Lhasa River	9	147.15	345.17	73.67	611.23
Jamuna River	5	1969.57	4327.59	341.52	13153.2	Lhasa River	10	97.64	271.52	30.07	928.31
Jamuna River	6	1442.33	4703.85	375.18	10848.79	Waitaki River	1	144.85	506.31	31.6	707.74
Jamuna River	7	1752.35	6655.06	315.06	16750.24	Waitaki River	2	126.53	396.37	32.55	829.75
Jamuna River	8	2615.38	4182.11	564.84	10239.98	Waitaki River	3	243.12	472.84	42.51	793.12
Jamuna River	9	1696.17	4762.69	587.74	15197.06	Waitaki River	4	78.64	226.06	21.75	522.2
Jamuna River	10	2444.77	7179.37	239.76	13604.84	Waitaki River	5	77.16	198.02	33.63	657.03
Rakaia River	1	233.97	460.72	39.4	1036.62	Waitaki River	6	233.24	652.93	45.21	999.75
Rakaia River	2	199.68	896.19	44.51	1144.93	Waitaki River	7	115.97	346.03	60.15	812.54
Rakaia River	3	264.02	614.03	63.65	1266.95	Waitaki River	8	278.76	603.4	44.5	625.36
Rakaia River	4	312.97	755.12	60.2	1729.76	Waitaki River	9	106.28	321.6	76.47	641.35

Table 1: Continued.

Braided river name	Case	Width of braided bar (m)	Length of braided bar (m)	Width of channel (m)	Width of braided river (m)	Braided river name	Case	Width of braided bar (m)	Length of braided bar (m)	Width of channel (m)	Width of braided river (m)
Rakaia River	5	368.67	847.51	68.39	1187.12	Waitaki River	10	134.08	382.68	36.74	76.733
Rakaia River	6	316.97	886.65	58.18	1286.24	Brahmaputra River	1	328.62	1480.12	167.28	1960.52
Rakaia River	7	332.92	768.91	72.58	1208.08	Brahmaputra River	2	930.38	2247.98	158.1	2742.55
Rakaia River	8	194.53	663.05	54.29	845.18	Brahmaputra River	3	696.71	1681.16	89.98	3717.04
Rakaia River	9	352.07	1370.55	69.11	932.87	Brahmaputra River	4	480.28	1438.27	163.27	2257.85
Rakaia River	10	284.79	806.2	59.35	1346.91	Brahmaputra River	5	582.09	1933.89	188.92	4602.91
Ganges River	1	80.05	342.6	43	284.01	Brahmaputra River	6	400.77	932.57	178.88	2650.93
Ganges River	2	110.59	390.22	78.96	570.73	Brahmaputra River	7	396.17	1011.53	96.27	3669.36
Ganges River	3	63.84	231.74	42.35	694.95	Brahmaputra River	8	541.66	1568.2	128.39	3232.86
Ganges River	4	116.62	326.31	28.64	762.92	Brahmaputra River	9	424.06	1101.03	77.81	3492.82
Ganges River	5	136.79	406.94	30.05	726.86	Brahmaputra River	10	500.68	1593.82	170	2908.09

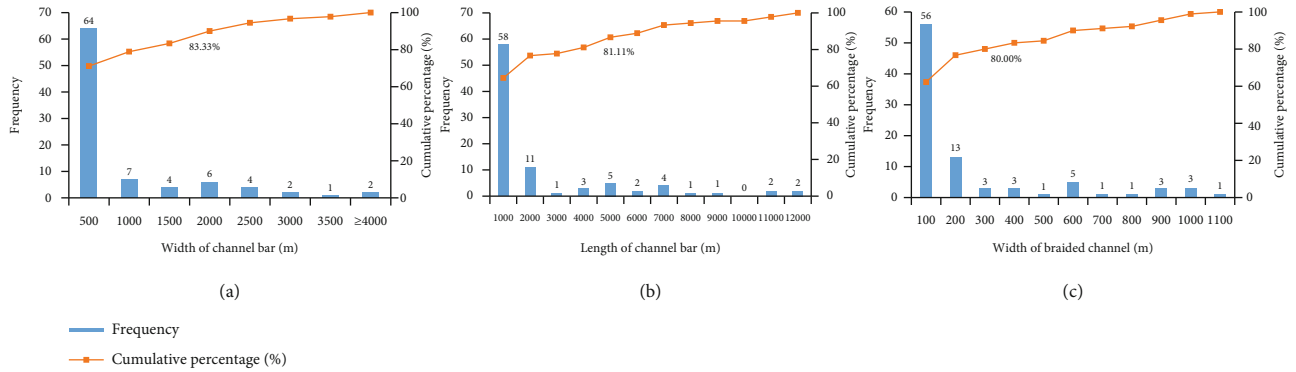

FIGURE 4: Probability distribution of different parameters based on a modern similar deposition. (a) Channel bar width, (b) channel bar length, and (c) braided channel width.

and the distance between the wells is approximately 600 m. We obtained the data related to exploration and production, such as core, logging curve, mud logging, seismic, sand interpretation, and other data types, from the Research Institute of Exploration and Development of North China Petroleum Bureau of Sinopec.

First, 9 typical sandy braided rivers were measured in planimetry using Google Earth software, and 10 sets of planimetric data were measured separately for each braided river, including the channel bars' lengths and widths, the braided channels' widths, and the braided rivers' widths. Second, 13 sets of profile data were measured for the target layer H1 using the digital outcrop dissection of Fugu Tianshengqiao, including the channel bars' and braided channels' widths and thicknesses. Finally, the results of 28 tank simulation experiments conducted at the Key Laboratory of Tank Simulation at Yangtze University enabled the counting of 84 groups of stable channel bar length and width data and 82 groups of detectable braided channel width data on a plane. From the 28 tank simulation experiments, 86 sets of channel bar width and thickness data and 91 sets of braided channel width and thickness data were statistically recorded in 12 tangential source profiles at various positions from the source.

Tank simulation experiments were completed in the Key Laboratory of Tank Simulation at Yangtze University. The research object is the sandy braided river deposits developed in the Daniudi gas field, Ordos Basin. The experimental site is 10 m long, 2.2 m wide, and 2 m deep. It primarily comprises a testbed, sediment screening equipment, constant speed water supply, sand supply equipment, a 3D laser scanner, and video recording equipment. Considering the depositional law of a braided river reservoir, experimental purposes, and measured data from the mainstream of the Yellow River's Huayuankou section with comparable depositional dynamics, it is demonstrated that the depositional slope of the braided river is 0.0267 m/10 m, the median grain size of the sediment is 0.2 mm, and the average velocity is 0.4–0.8 m/s. The primary tank simulation parameters were determined using the hydrological data from the Yellow River's Huayuankou section. The slope was 0.1 m/10 m, and the median grain size of the sediment was 0.3 mm (the sand composition comprised green and yellow sand in a 3 : 1 ratio). The average velocity was 0.25 m/s.

The geological knowledge database-based braided river modeling proposed in this paper is based on a combination of similar modern sedimentation, field outcrop profiles, and tank simulation experiments to analyze the quantitative relationship between the microfacies of braided channels and channel bars in planes and profiles. Furthermore, the different microfacies thicknesses were divided in the wells in the study area. Establishing a quantitative geological knowledge database of the braided river reservoir's microfacies was guided and applied to a 3D geological model of the H1 member to identify simulation parameters. The 3D training images were simulated using the object-based method, and a sedimentary facies model was built using the multiple-point geostatistical modeling method. The study area is divided into 25 × 25 m grids in the plane and 0.5 m grids vertically, totaling 89,478,400 grids.

4. Results

4.1. Similar Modern Depositional Statistics. Google Earth software was used to screen nine typical modern sandy braided rivers with similar depositional backgrounds to the study area, including the Ningxia part of the Yellow, Lena, and Jamuna Rivers (Figure 3), and 10 sets of channel bar length and width and braided channel width data were measured for each river (Table 1). According to the statistics, the widths of sandy braided river channel bars are below 1500 m, with 16.67% exceeding 1500 m, and the average width is approximately 675 m (Figure 4(a)). The channel bar lengths are primarily less than 4000 m, with 18.89% over 4000 m, and the average length is approximately 1965 m (Figure 4(b)). The active braided channel widths are typically less than 300 m, with 20% surpassing 300 m, and the average width is approximately 195 m (Figure 4(c)).

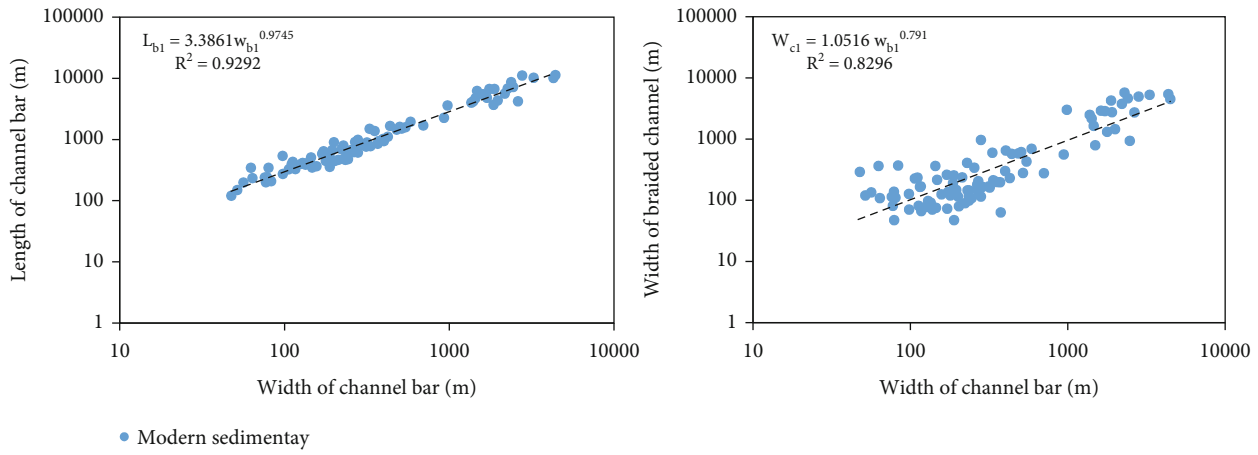

FIGURE 5: Correlation between different parameters of modern similar deposits: (a) the length of the channel bar and its width; (b) the width of the braided channel and channel bar.

FIGURE 6: Identification of braided river architecture based on the digital outcrop model. (a) Tianshengqiao outcrop, Fugu county, Ordos Basin; (b) typical lithofacies types of braided river deposits in the H1 member; (c–f) braided river scale measurement; (g)–(j) channel bar scale measurement.

Linear regression analysis was conducted for 90 parameter sets, including channel bar length and width and channel bars and braided channel widths, to analyze the scale of the sand body parameters quantitatively, and the results were positively and well correlated (Figure 5). The relationship between the length of the channel bar (l_{b1}) and its width (w_{b1}), the width of the braided channel (w_{c1}), and the width of the channel bar (w_{b1}) was established for modern sandy braided rivers.

$$\begin{aligned} l_{b1} &= 3.3861 w_{b1}^{0.9745}, \\ w_{c1} &= 1.0516 w_{b1}^{0.791}, \end{aligned} \tag{1}$$

Table 2: Statistics of digital field outcrop channel bar and braided channel scale parameters.

Microfacies types	Real measurement width (m)	Estimate real width (m)	Thickness (m)	Microfacies types	Real measurement width (m)	Estimate real width (m)	Thickness (m)
Channel	55.29	138.225	9.38	Small braided bar	56.82	113.64	5.47
Channel	133.9	200.85	8.85	Small braided bar	115.02	287.55	6.63
Channel	39.7	39.7	4.56	Small braided bar	33.78	33.78	8.75
Channel	61.71	123.42	6.49	Small braided bar	32.7	32.7	4.31
Channel	45.42	45.42	5.48	Small braided bar	161.01	161.01	11.37
Channel	42.73	128.19	11.11	Large braided bar	127.66	319.15	5.63
Channel	85.01	85.01	12.04	Large braided bar	256.41	897.435	14.11
Channel	55.3	55.3	4.92	Large braided bar	194.61	681.135	11.89
Channel	85.6	85.6	4.56	Large braided bar	325.53	976.59	17.95
Channel	44.69	44.69	6.65	Large braided bar	304.24	608.48	8.18
Channel	63.5	63.5	12.17	Large braided bar	181.21	724.84	16.65
Channel	55.04	55.04	6.05	Large braided bar	418.69	837.38	10.98
Channel	31	31	3.8	Large braided bar	137.06	548.24	20.66

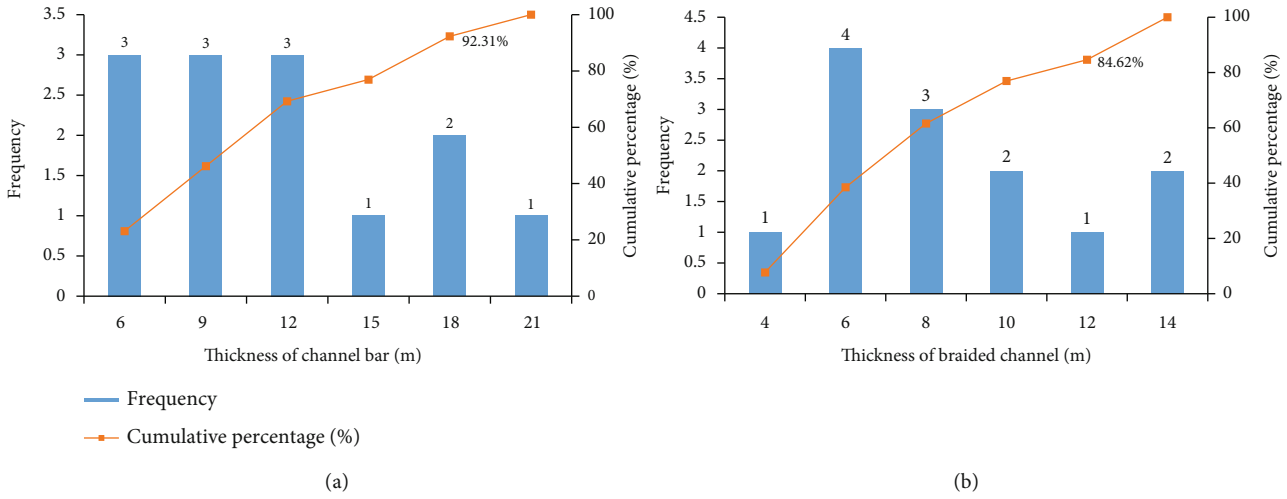

Figure 7: Probability distribution of different parameters based on the digital field outcrop. (a) Thickness of the channel bar; (b) thickness of the braided channel.

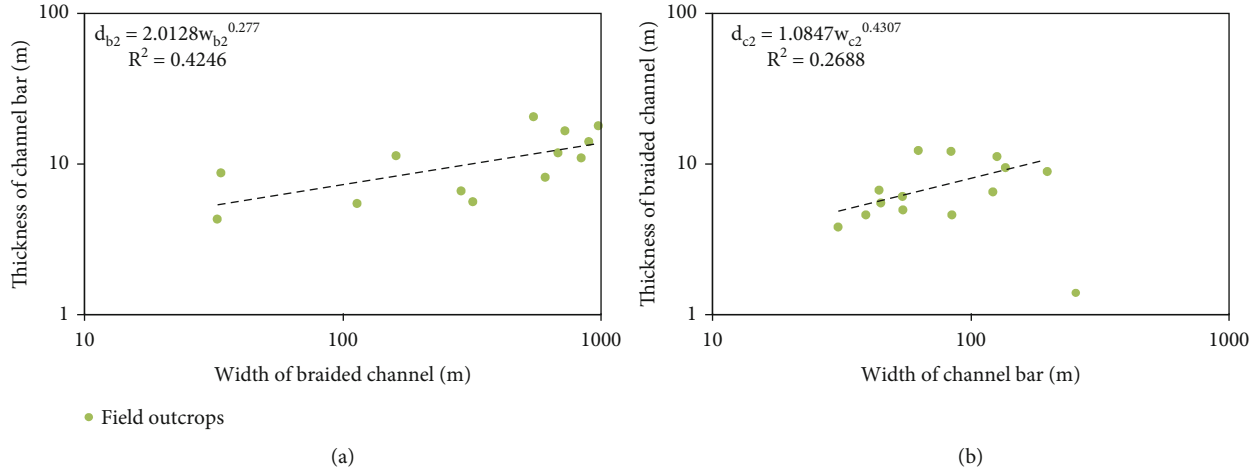

Figure 8: Correlation between different parameters of digital field outcrops. (a) The length of the channel bar and its width; (b) the width of the braided channel and channel bar.

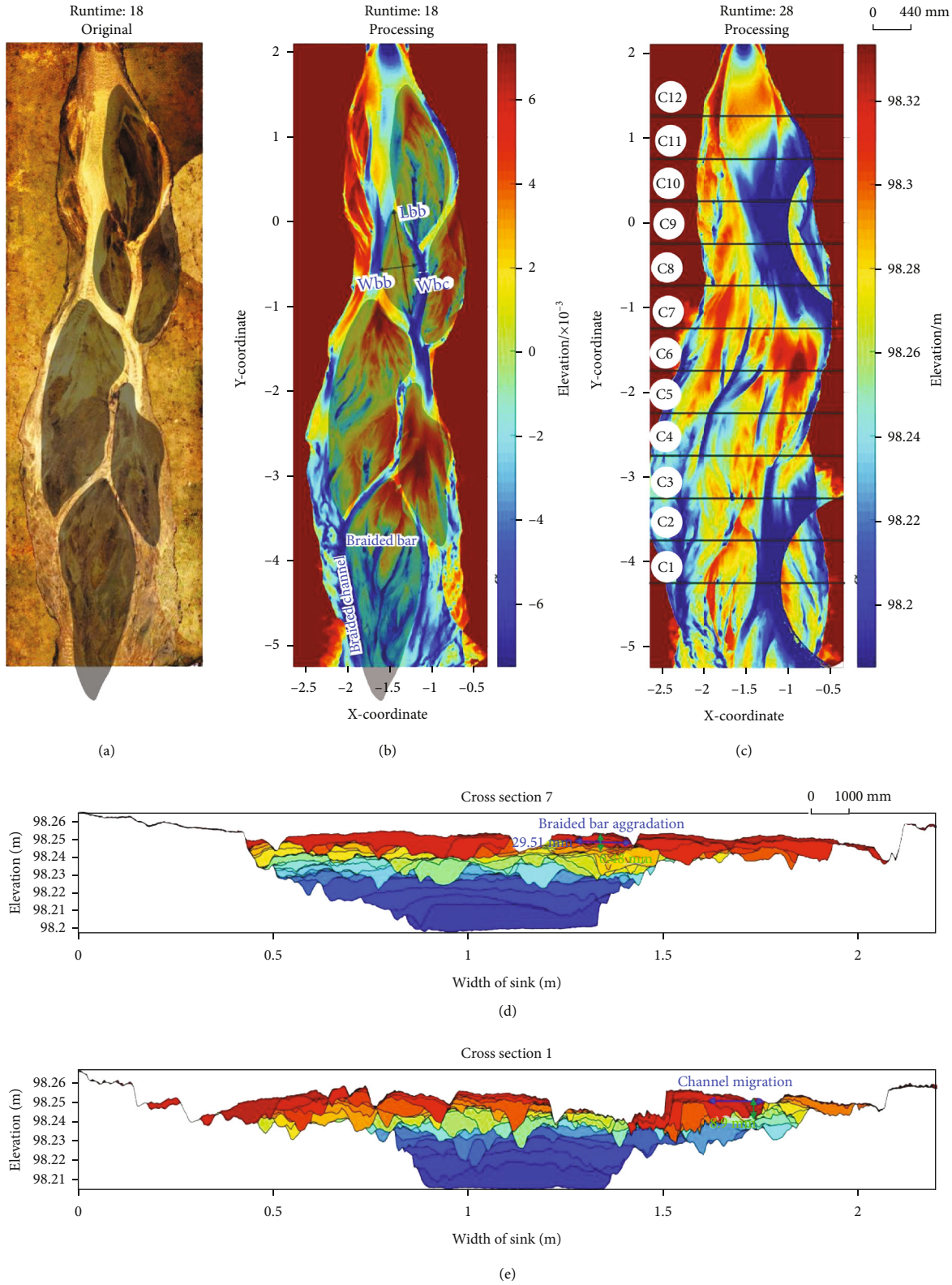

FIGURE 9: Identification of braided river architecture based on tank simulation experiments. (a) Tank simulation experiments in phase 18; (b) the 18th detrending to emphasize the shape and spreading features of the braided river, (c) the 28th detrending to emphasize the shape and spreading features of the braided river and profile locations, (d) experimental profile C7 of phase 28, (e) experimental profile C1 of phase 28. Wbb: width of braided bar; Lbb: length of braided bar; Wbc: width of braided channel; C12: cross section 12; C11: cross section 11; C10: cross section 10; C9: cross section 9; C8: cross section 8; C7: cross section 7; C6: cross section 6; C5: cross section 5; C4: cross section 4; C3: cross section 3; C2: cross section 2; C1: cross section 1.

Table 3: Statistics of tank simulation experimental channel bar and braided channel plane scale parameters.

Simulation phase	Braided bar		Width of braided channel (mm)	Simulation phase	Braided bar		Width of braided channel (mm)	Simulation phase	Braided bar		Width of braided channel (mm)	Simulation phase	Braided bar		Width of braided channel (mm)
	Width (mm)	Length (mm)			Width (mm)	Length (mm)			Width (mm)	Length (mm)			Width (mm)	Length (mm)	
11	31.22	75.88	3.79	14	42.79	140.4	6.64	18	26.85	85.1	2.89	24	36.72	107.66	1.44
11	31.25	92.7	2.17	14	17.77	87.11	2.2	18	38.66	114.52	8.39	24	19.91	115.29	4.56
11	33.01	109.87	3.15	14	25.91	72.57	3.86	19	41.17	133.43	3.14	24	19.83	68.07	4.44
11	30.06	107.61	6.43	15	23.44	111.3	3.85	19	23.43	85.52	3.55	24	32.89	110.24	3.75
11	20.77	89.85	4.51	15	30.02	168.32	5.72	19	39.15	107.89	7.2	24	21.53	65.7	4.25
11	38.67	131.79	7.03	15	60.93	157.37	6.99	20	30.08	92.51	3.67	24	41.58	149.53	3.19
12	32.51	77.15	4.03	15	31.57	81.47	4.56	20	44.95	167.56	7.34	25	32.8	113.06	2.64
12	26.25	96.7	—	16	22.17	94.2	2.98	20	31.81	97.88	4.18	25	44.31	115.9	4.07
12	26.91	113.44	4.15	16	19.67	97.12	5.53	20	26.8	127.08	4.07	25	53.33	138.5	8.9
12	33.2	94.99	3.31	16	24.09	109.19	2.49	21	58.45	134.02	5.87	25	34.55	156.93	6.75
12	18.71	92.68	3.36	16	55.46	145.83	6.27	21	27.83	128.03	7.51	26	37.36	104.62	6.58
12	26.32	81.22	6.63	16	30.59	69.84	6.94	21	57.13	142.14	7.64	26	32.03	131.78	3.23
12	14.51	58.21	—	17	25.18	125.4	3.07	22	33.47	123.89	5.51	26	42.66	114.58	7.15
13	32.2	105.17	6.15	17	17.96	62.86	6.51	22	31.38	77.6	2.47	26	32.02	89.43	6.46
13	31.61	139.34	2.48	17	53.08	118.2	6.08	22	39.71	200.13	2.06	27	40.2	100.91	2.84
13	21.43	68	3.13	17	39.5	105.73	5.87	22	27.96	98.81	5.04	27	44.41	145.76	6.58
13	16.31	68.1	2.66	17	28.36	74.95	5.16	22	24.17	96.08	6.7	27	23.01	95.23	2.55
13	23.26	92.44	4.16	18	30.02	79.75	2.77	23	19.8	82.7	6.25	27	34.04	99.86	4.66
13	22.53	87.12	4.78	18	19.86	73.14	4.87	23	34.98	98.09	4.19	28	38.41	165.15	3.4
14	38.6	108.33	4.95	18	19.64	55.43	4.21	23	53.86	184.02	6.12	28	25.48	74.42	2.47
14	32.4	113.64	5.84	18	38.25	112.39	4.47	23	24.88	88.03	2.6	28	36.79	151.94	3.52

Table 4: Statistics of tank simulation experiment channel bar and braided channel profile scale parameters (the location of the profile can be seen in Figure 9(c)).

(a)

Section position	Width of braided channel (mm)	Thickness of braided channel (mm)	Section position	Width of braided channel (mm)	Thickness of braided channel (mm)	Section position	Width of braided channel (mm)	Thickness of braided channel (mm)	Section position	Width of braided channel (mm)	Thickness of braided channel (mm)
C1	32.68	10.42	C3	43.82	10.64	C6	26.32	4.02	C9	17.63	6.91
C1	8.55	4.64	C3	36.54	10.16	C6	28.65	7.81	C9	23.68	7.73
C1	22.72	10.8	C4	18.03	17.78	C6	24.67	3.92	C9	13.89	8.16
C1	26.94	11.29	C4	18.17	5.25	C6	44.57	20.01	C9	20	10.85
C1	12.91	8.94	C4	13.08	3.94	C6	32.64	8.74	C9	25.06	8.78
C1	23.04	10.75	C4	22.6	10.69	C6	25.62	8.15	C9	12.12	7.66
C1	23.07	13.13	C4	25.67	13.34	C6	17.73	11.06	C9	25.84	10.64
C1	8.75	7.2	C4	52.3	11.54	C7	29.32	8.26	C9	38.55	18.13
C1	14.04	10.01	C4	22.21	6.04	C7	13.65	5.96	C10	40.56	7.81
C1	15.75	8.31	C4	27.8	10.11	C7	38.52	8.31	C10	9.13	3.29
C2	30.85	13.44	C5	8.11	3.47	C7	19.16	5.63	C10	24.66	5.87
C2	19.62	15.46	C5	7.82	3.02	C7	28.47	7.15	C10	25.6	6.69
C2	27.63	13.42	C5	9.82	3.97	C7	17.63	7.67	C10	17.28	6.99
C2	12.72	6.4	C5	19.91	8.48	C7	29.32	11.54	C10	10.14	4.56
C2	20.7	5.72	C5	22.82	7.47	C7	11.29	5.98	C11	12.81	6.49
C2	17.42	10.26	C5	31.72	17.38	C7	25.75	4.77	C11	13.31	5.51
C2	43.01	14.91	C5	19.26	7.67	C8	19.88	10.69	C11	13.45	3.81
C2	26.59	13.61	C5	23.19	10.49	C8	18.81	7.36	C11	49.43	10.54
C2	12.14	8.9	C5	19.27	4.52	C8	26.2	9.16	C11	17.45	5
C3	22.56	13.87	C5	22.76	8.08	C8	31.41	7.14	C12	9.63	7.14
C3	22	5.79	C6	17.36	3.56	C8	39.03	16.3	C12	17.61	11.59
C3	24.55	5.95	C6	35.03	7.76	C8	22.86	16.35	C12	14.6	3.86
C3	13.82	10.64	C6	20.01	6.51	C9	28.58	10.9			

(b)

Section position	Width of channel bar (mm)	Thickness of channel bar (mm)	Section position	Width of channel bar (mm)	Thickness of channel bar (mm)	Section position	Width of channel bar (mm)	Thickness of channel bar (mm)	Section position	Width of channel bar (mm)	Thickness of channel bar (mm)
C1	17.03	3.68	C3	47.18	4.95	C6	23.68	6.46	C9	22.39	4.98
C1	37.47	11.11	C4	61.55	10.22	C6	25.24	5.09	C10	48.51	3.97
C1	51.35	6.09	C4	46.75	9.26	C6	31.67	4.6	C10	34.91	8.79
C1	26.35	6.89	C4	17.81	2.21	C6	125.8	11.85	C10	58.83	7.31
C1	21.88	8.41	C4	44.27	5.93	C6	38.96	1.85	C10	29.62	4.02
C1	38.82	6.67	C4	70.91	5.14	C7	116.33	9.21	C10	15.93	6.36
C1	40.2	6.41	C4	32.57	7.44	C7	25.3	5.93	C10	19.78	3.3
C1	23.78	8.1	C4	41.17	6.54	C7	29.51	6.78	C11	21.57	4.66
C1	27.89	6.25	C4	65.83	2.12	C7	121.32	13.23	C11	34.39	5.9
C2	22.17	5.82	C5	14.31	4.52	C8	81.51	7.83	C11	61.48	7.52
C2	29.9	9.44	C5	82.77	4.5	C8	41.28	3.2	C11	56.14	4.55
C2	49.8	10.64	C5	50.59	6.83	C8	25.43	3.25	C11	38.27	6.46
C2	60.61	11.28	C5	45.03	2.37	C8	22.66	3.94	C11	32.58	3.83
C2	37.29	8.89	C5	25	4.02	C8	37.73	7.14	C11	26.22	2.7
C2	35.9	7.92	C5	14.71	2.98	C8	23.83	4.74	C11	32.13	5.35

Table 4: Continued.

Section position	Width of channel bar (mm)	Thickness of channel bar (mm)	Section position	Width of channel bar (mm)	Thickness of channel bar (mm)	Section position	Width of channel bar (mm)	Thickness of channel bar (mm)	Section position	Width of channel bar (mm)	Thickness of channel bar (mm)
C2	33.68	5.82	C5	29.32	3.65	C8	26.32	4.34	C11	17.81	3.81
C2	30.27	5.19	C5	20.97	4.1	C8	33.23	6.51	C12	68.16	6.78
C3	56.26	6.06	C5	70.59	7.31	C9	65.55	6.09	C12	81.44	8.26
C3	45.79	12.22	C5	20.15	2.33	C9	70.07	8.26	C12	36.14	6.02
C3	65.23	11.86	C6	9.67	2.37	C9	29.58	8.44	C12	53.9	8.47
C3	71.15	12.81	C6	14.21	2.78	C9	20.67	4.4	C12	44	4.66
C3	31.2	5.08	C6	74.63	9.31						

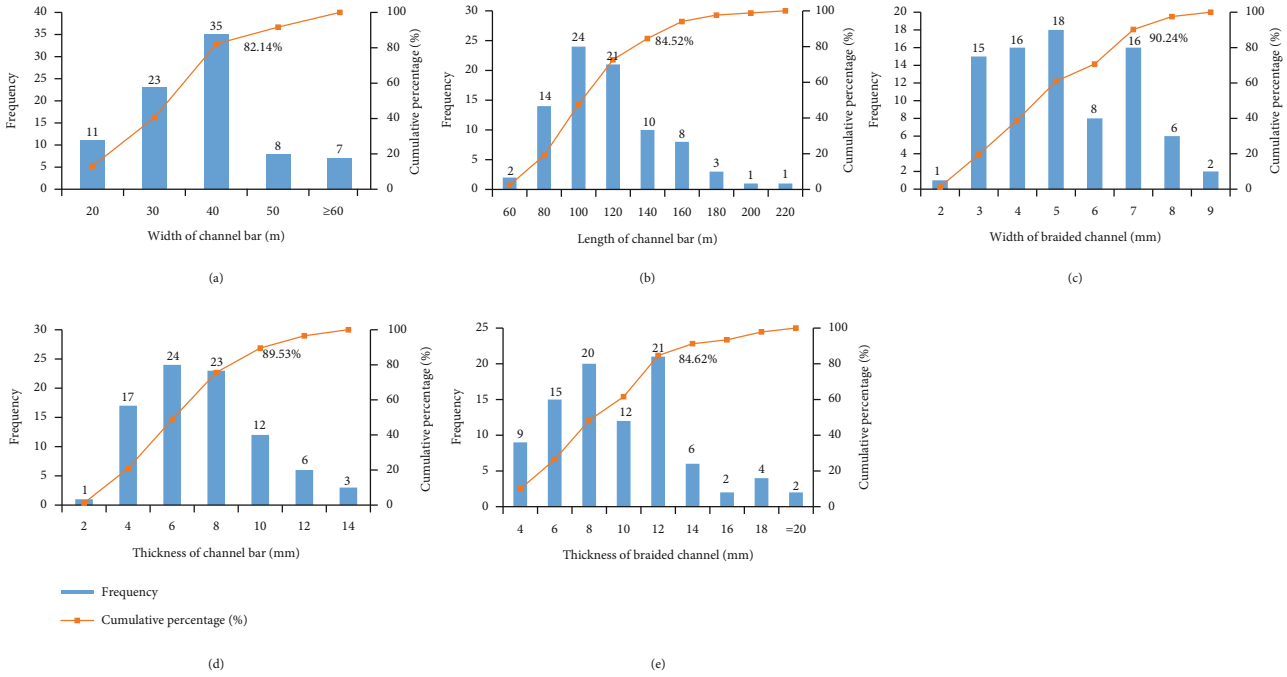

Figure 10: Probability distribution of different parameters based on the tank simulation experiments. (a) Width of the channel bar, (b) length of the braided channel, (c) width of the braided channel, (d) thickness of the channel bar, and (e) thickness of the braided channel.

where l_{b1} is the length of modern sedimentary channel bars (m), w_{b1} is the width of modern sedimentary channel bars (m), and w_{c1} is the width of modern sedimentary braided channels (m).

4.2. Digital Outcrop Statistics. Field outcrop profiling is the primary technical method for obtaining geometric shapes and scale data of braided channels and channel bars [36]. Even though outcrops are restricted and cannot provide a complete characterization of sedimentary structures (e.g., braided river width), they include a wealth of information on the architectural elements of braided river reservoirs [37]. The Fugu Tianshengqiao outcrop has the same target formation, depositional environment, and reservoir characteristics as the Daniudi gas field in this subsurface research region. The outcrop sections evolve from the bottom up in the Ordovician Majiagou, Carboniferous Benxi, Taiyuan, Permian Shanxi, and Lower Shihezi Formations [33]. The average elevation of the surface is 813 m, the height of the outcrop is 30–100 m, the primary body of the outcrop is trending northeast–southwest, the stratigraphic tendency is 280°, the dip angle is 4°–10°, and the sand body is visible in different directions, convenient for sand body lateral tracing and comparison and fine internal dissection.

The Fugu Tianshengqiao architecture's anatomy is based on the digital outcrop model (Figure 6(a)), microfacies division (Figure 6(b)), and precise measurement of the channel bar and braided channel sands on the profile (Figures 6(c)–6(j)). For the target layer H1, 13 sets of

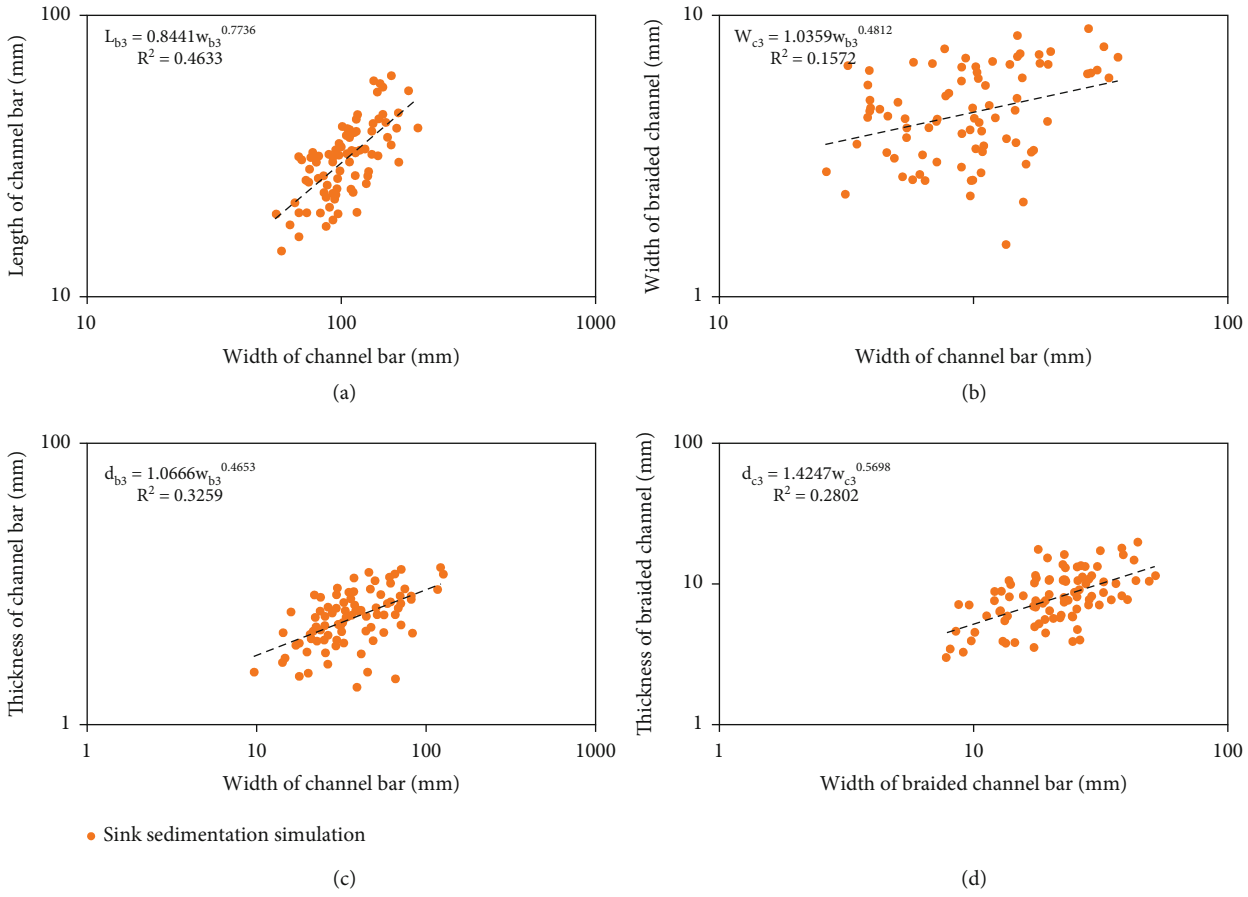

Figure 11: Correlation between different parameters of tank simulation experiments. (a) The length of the channel bar and its width, (b) the width of the braided channel and channel bar, (c) the thickness of the channel bar and its width, and (d) the thickness of the braided channel and its width.

channel bar width and thickness and braided channel width and thickness data (Table 2) were measured individually (the scale of the incomplete sand body was estimated for the outcrop). According to the outcrop data statistics, single minor channel bars are 30–300 m wide, whereas major composite channel bars are 300–1000 m wide and 6–21 m thick, with an average thickness of approximately 11 m, and only 7.69% of channel bars are more than 18 m thick (Figure 7(a)). The braided channels were 30–200 m wide and 4–14 m thick, with an average thickness of approximately 7.5 m, and only 15.38% of the braided channels were deeper than 12 m (Figure 7(b)).

Linear regression analysis was performed on 13 parameters, including channel bar widths and thicknesses and braided channel widths and thicknesses. The results were positively correlated, although the correlation was poor (Figure 8) because some strata are incompletely exposed or extensively denuded (Figures 6(a) and 6(e)). The scale and quantitative relationship between channel bars and braided channel profiles have been established using digitized outcrop modeling. The following shows the correlation between the channel bar thickness (t_{b2}) and its width (w_{b2}) (Figure 8(a)) and the thickness of the braided channel (t_{c2}) and its width (w_{c2}) (Figure 8(b)) in the field outcrop.

$$t_{b2} = 2.0128w_{b2}^{0.277},$$
$$t_{c2} = 1.0847w_{c2}^{0.4307}, \quad (2)$$

where t_{b2} is the thickness of the field outcrop channel bar (m), w_{b2} is the width of the field outcrop channel bar (m), $t_{c2}$is the thickness of the field outcrop braided channel (m), and w_{c2} is the width of the field outcrop braided channel (m).

4.3. Sink Simulation Experiments Statistics. Tank simulation experiments provide various reservoir sand models of varying depositional types [38–40]. These models resemble outcrops, modern sediments, and subsurface sediment bodies. The primary benefits include simple measurements (you can slice and sample at will), detailed records of depositional processes, and clear genesis mechanisms [41]. It is significant for sedimentology research and determining the reservoir's macroscopic distribution pattern parameters. We simulate the deposition of a braided river in the Lower Shihezi Formation of the Daniudi gas field with the same

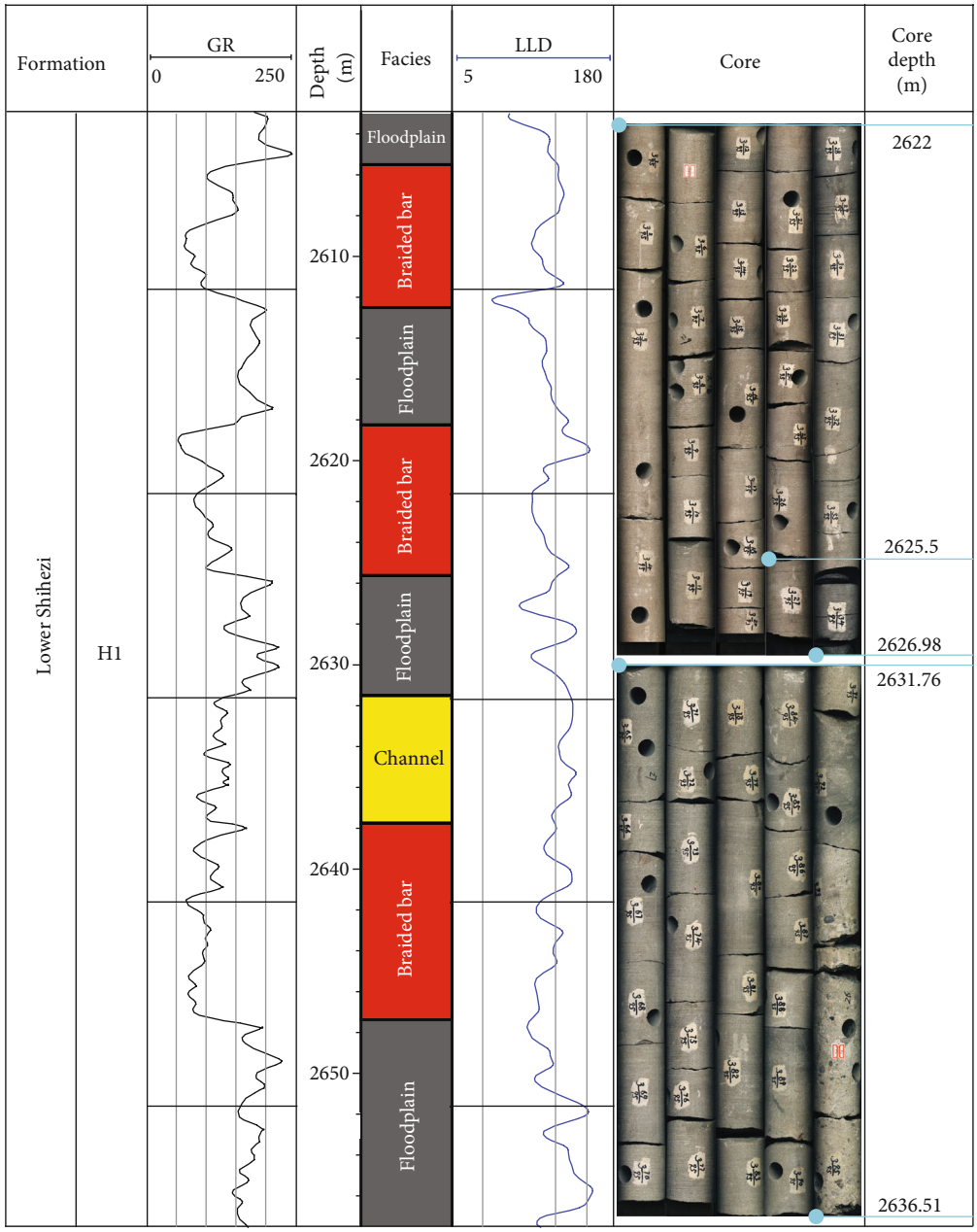

Figure 12: Lithology and facies interpretation based on core and logging curve data of well D.

parameters of sediment grain size, hydrodynamic conditions, and slope drop as the reservoir in the research area and a comparable depositional environment based on the principle of the *present being a key to the past*. The results of the tank simulation experiments in phase 18 (Figure 9(a)) were detrended to emphasize the shape and spreading features of the braided channel and the channel bar (Figure 9(b)) by integrating the 28-phase tank simulation process. As the experiments increased, the channel bar gradually changed from a long elliptical shape with a single style to a wide-short elliptical composite channel bar with a complex internal structure (Figures 9(b) and 9(c)). The parameters of a stable channel bar and braided channel in the experiments simulated after phase 11 were measured (Figure 9(b)), and 84 channel bar length and width data and 82 channel bar to braided channel width ratio data were statistically recorded on the plane (Table 3). Figure 9(d) shows the vertical accretion process of the composite channel bar, and Figure 9(e) shows the migration process of the braided channel. In total, 86 sets of channel bar width–thickness ratio data and 91 sets of braided channel width–thickness ratio data were statistically recorded (Table 4). In the profile, data on the composite channel bar and braided channel width–thickness were collected in phase 28 at 12 cut source locations.

According to the statistics of the tank simulation experimental planes and profiles, the stable channel bar's width is between 20 and 60 mm, with an average width of 32 mm,

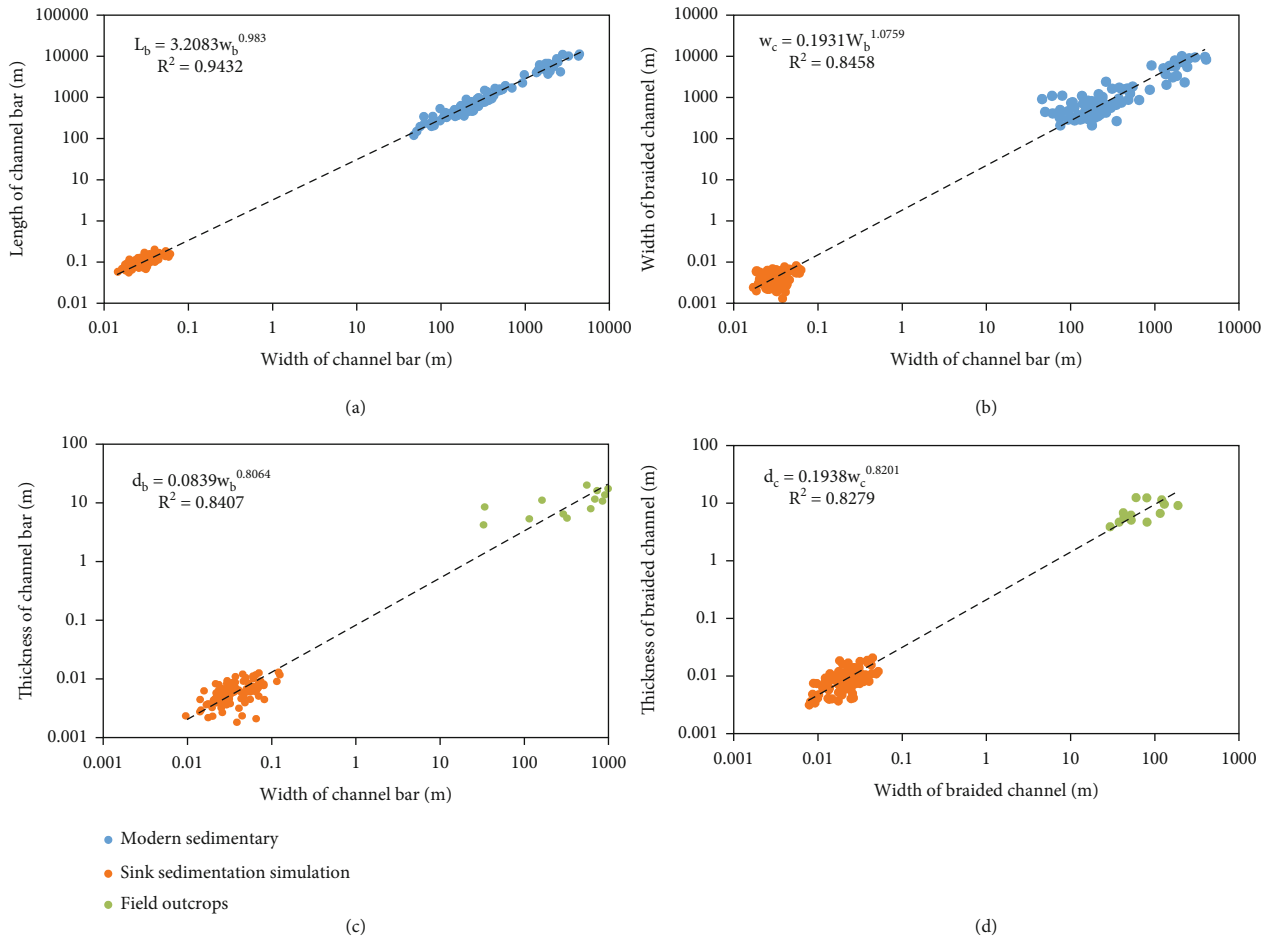

FIGURE 13: Quantitative relationships between modern sedimentation, field outcrops, and tank simulation experimental parameters. (a) The channel bar's length and width with modern sedimentation and tank simulation experiments on planes, (b) the width of the braided channel and channel bar with modern sedimentation and tank simulation experiments on planes, (c) the channel bar's thickness and width with field outcrops and tank simulation experiments on profiles, and (d) the braided channel's thickness and width with field outcrops and tank simulation experiments on profiles.

and only 17.86% is wider than 40 mm (Figure 10(a)). The channel bar's length was between 60 and 220 mm, with an average length of 107 mm, and only 15.48% were greater than 140 mm (Figure 10(b)). The active braided channel's width was 2–9 mm, with an average braided channel width of 4.6 mm, and only 9.76% were wider than 7 mm (Figure 10(c)). The channel bar thickness was 2–14 mm, with an average of 6.3 mm, and only 10.47% exceeded 7 mm (Figure 10(d)). The active braided channel thickness was 4–20 mm, with an average braided channel thickness of 8.8 mm, and only 15.38% were more than 12 mm (Figure 10(e)).

Linear regression analyses of stable channel bar lengths and widths, channel bar widths and thicknesses, channel bar widths and braided channel widths, and braided channel widths and thicknesses were performed. However, the correlation results were poor. Based on the tank simulation experiments, the scale and quantification of the relationship between the channel bar and the braided channel in planes and profiles were established. Furthermore, the relationships between the length of the channel bars l_{b3} and its width w_{b3} (Figure 11(a)), the width of the braided channel w_{c3}, the width of the channel bar w_{b3} (Figure 11(b)), the thickness of the channel bar t_{b3} and its width w_{b3} (Figure 11(c)), and the thickness of the braided channel t_{c3} and its width w_{c3} (Figure 11(d)) were obtained.

$$\begin{aligned} l_{b3} &= 0.8441 w_{b3}^{0.7736}, \\ w_{c3} &= 1.0359 w_{b3}^{0.4182}, \\ t_{b3} &= 1.0666 w_{b3}^{0.4653}, \\ t_{c3} &= 1.4247 w_{c3}^{0.5698}. \end{aligned} \tag{3}$$

Here, l_{b3} is the length of the tank simulation experiment's channel bar (m), w_{b3} is the width of the tank simulation experiment's channel bar (m), w_{c3} is the width of the tank simulation experiment's braided channel (m), t_{b3} is the thickness of the tank simulation experiment's channel bar (m), and t_{c3} is the thickness of the tank simulation experiment's braided channel (m).

Table 5: Quantitative knowledge database of the braided river in the Lower Shihezi Formation of the Daniudi gas field.

Member	Braided channel		Channel bar					
			Single minor channel bar			Major composite channel bar		
	Thickness (m)	Width (m)	Thickness (m)	Width (m)	Length (m)	Thickness (m)	Width (m)	Length (m)
H1	1-22	7-320	3-9	80-330	240-1000	9-30	330-1500	1000-4200

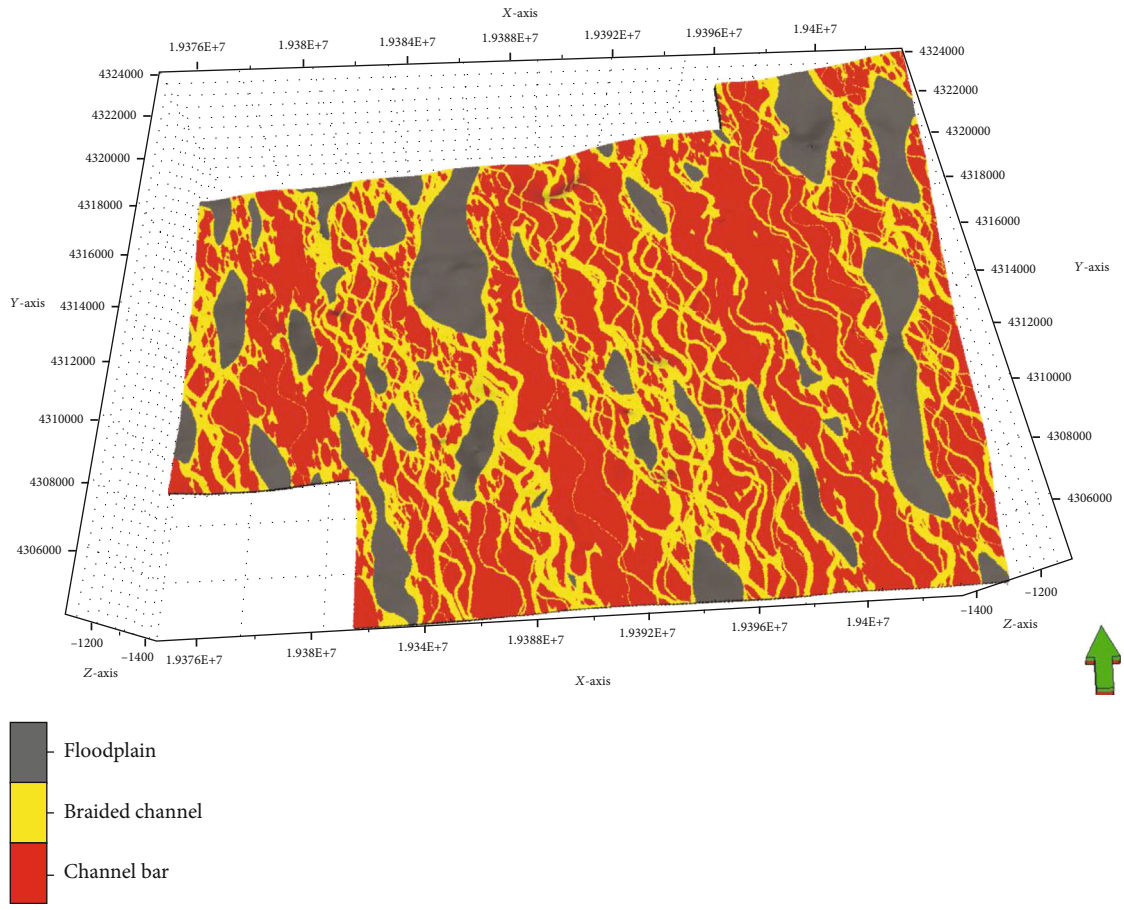

Figure 14: 3D training images of braided river reservoirs in the Daniudi gas field based on a quantitative geological knowledge database.

4.4. Microfacies Classified Based on Well Data. The primary development member of the Daniudi gas field, H1, is a sandy braided river system with box-shaped and bell-shaped gamma-ray (GR) logging curves produced in the primary part of the braided river (Figure 12). The bell-shaped GR log curve, with the bottom in abrupt contact with the underlying strata, relates to bottom scouring, and the top is in gradual contact with mudstone, reflecting progressively weakening hydrodynamic characteristics, and its corresponding sedimentary microfacies is a braided channel. The top and bottom of the smooth box-shaped GR log curve abruptly contact the mudstone, reflecting strong and stable hydrodynamic characteristics of sufficient material sources. The jagged box-shaped GR log curve reflects strong but unstable hydrodynamic conditions, with frequent alternations of strength and weakness, and its corresponding sedimentary microfacies is a channel bar. The channel bar's thickness is 3–30 m, and the thickness of the braided channel is 1–22 m, according to the measurement statistics of the underground core well data of the Daniudi gas field.

4.5. Quantitative Knowledge Database of a Sandy Braided River Reservoir in Daniudi. Popular methods in reservoir geological knowledge database investigations include modern sedimentation, outcrop anatomy, and dense well network dissection. A comparison of empirical formulas for modern sedimentation, outcrop anatomy, and tank simulation data reveals that planimetric data based on modern sedimentation has the best correlation; however, measurement statistics have poor correlations due to the outcrops on the exposed surface affected by denudation, tank simulation experimental sites, and other factors. Therefore, the results of modern sedimentation, outcrop surveys, and tank simulation experiments are corroborated to establish a geological knowledge database for reservoir parameter prediction. All measurements were combined, and correlations between

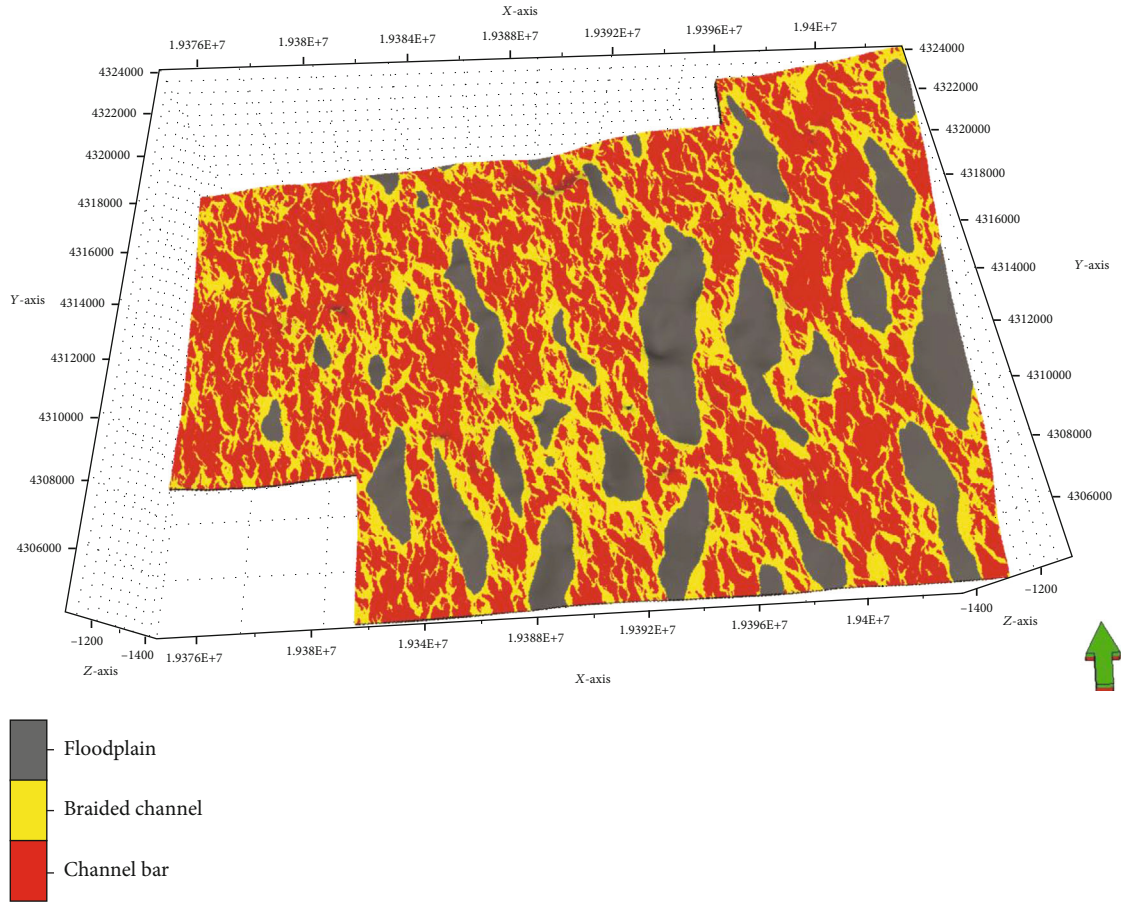

FIGURE 15: Multiple-point geostatistical model based on subsurface well data in Daniudi and training images using the database.

modern sedimentation and tank simulation experiments on planes (Figures 13(a) and 13(b)) and field outcrops and tank simulation experiments on profiles (Figures 13(c) and 13(d)) were fitted, respectively.

The measured data from the tank simulation experiments on planes and profiles are compared to planimetric data from modern sedimentation measurements and profile data from field outcrop observations. When relating the tank simulation experiments to modern deposition data on a plane, the quantitative relationship between the channel bar length and width is $l_b = 3.2083 w_b^{0.983}$ (9), with correlation $R^2 = 0.9432$—the results are highly correlated (Figure 13(a)). The quantitative relationship between the braided channel and channel bar width is $w_c = 0.1931 w_b^{1.0759}$ (10), with a correlation of $R^2 = 0.8458$, which correlated well (Figure 13(b)). When relating the tank simulation experiments to field outcrop anatomical data on the profile, the quantitative relationship between channel bar thickness and width is $t_b = 0.0839 w_b^{0.8064}$ (11), showing a good correlation of $R^2 = 0.8407$ (Figure 13(c)). The quantitative relationship between river thickness and width is $t_c = 0.1938 w_c^{0.8201}$ (12), a decent correlation of $R^2 = 0.8279$ (Figure 13(d)). The correlations of all four data sets increased, indicating that the quantitative relationships obtained after integrating the data from modern sedimentation, field outcrop, and tank simulation experiments are real and reliable and can guide establishing a quantitative knowledge database of sandy braided river reservoirs in the Daniudi gas field.

Based on the anatomical understanding of the reservoir sand thickness in the Daniudi gas field, Ordos Basin (Figure 12), combined with a similar modern deposition of the braided river, field outcrop, and tank simulation experiments, a quantitative equation of parameters was fitted (Figure 13). Each sedimentary microfacies unit's scale of parameters in the study area, such as thickness, width, and length, was determined, and the quantitative geological knowledge database of the sandy braided river in the Lower Shihezi Formation of the Daniudi gas field was established (Table 5). The braided channel has a thickness of 1–22 m and a width of 7–320 m. The single minor channel bar has a thickness of 3–9 m, a width of 80–330 m, and a length of 240–1000 m, and the major composite channel bar has a thickness of 9–30 m, a width of 330–1500 m, and a length of 1000–4200 m.

5. MPS Simulation Using Training Images from Geological Knowledge Database

5.1. Training Image Generation. The multiple-point algorithm can realistically depict the morphology of complex geological bodies while remaining faithful to the original

data [42]. The training image is used instead of the traditional variation function to express the correlation between multiple points in space when using the multiple-point geostatistical modeling method for simulation. The training images can show the real reservoir structure, geometry, contact relationships, distribution patterns, and geological knowledge database information in 3D space and reproduce geologists' geological understanding of the research area. Creating training images includes hand-drawn, object-based simulation; 3D seismic information extraction or transformation; prototype-based models; process-based simulations; and 2D image methods [43]. However, the reliability of the training images limits the accuracy of the simulation results, with the primary issue being a scarcity of 3D training images appropriate for the research area.

A realistic and credible 3D training image is constructed using a quantitative approach that integrates modern sedimentation, outcrop profile, and tank simulation experimental database simulations with drilling data and using the object-based method (Figure 14). According to the statistics of subsurface well data from the Daniudi gas field, the training images include the floodplain (19.02%), the braided channel (36.15%), and the channel bar (44.83%). The generated training images can realistically reproduce a 3D morphology of the reservoir by describing the morphology of the sand body, such as its length, width, thickness, and quantitative correlations. 3D training images show the migrating superposition variants of braided channels and channel bars in the plane and longitudinal directions.

5.2. MPS Realization. The established geological model can only be close enough to the real characteristics of subsurface sedimentary bodies by applying the quantitative geological knowledge database of braided rivers established in the previous stage to a 3D geological modeling of the Lower Shihezi Formation in the Daniudi gas field. Through the creation of 3D training images, the multiple-point geostatistical modeling method defines the model's reservoir distribution and sand body structure and achieves results that characterize the actual geometry and quantitative relationships of the subsurface sediment bodies (Figure 15). The results of the model simulated using multiple-point geostatistical method are compared with the hard data in the well, and the well conditioning can reach 100%.

6. Conclusions

(1) The frequency and distribution intervals of various sedimentary microfacies parameters of a braided river reservoir were analyzed using modern statistical sedimentation, field outcrop, and tank simulation experiments. By fitting the relationship between the parameters, the length and width of the channel bar, the width of the braided channel and channel bar, the thickness and width of the channel bar, and the thickness and width of the braided channel positively correlated to exponential power relationships

(2) A quantitative knowledge database of braided river sedimentary microfacies applicable to the Lower Shihezi Formation of the Daniudi gas field was established, with single-phase braided channel thicknesses of 1–22 m, widths of 7–320 m, and channel bar thicknesses of 3–30 m, widths of 80–1500 m, and lengths of 240–4200 m

(3) For the Daniudi gas field, a 3D geological modeling method is proposed that is compatible with the advantages of object-based and multiple-point methods. The established 3D training images characterize the depositional features of the braided river reservoir and the results of geological knowledge database research, allowing the final geological model results to characterize the real geometry and quantitative relationships of subsurface sedimentary bodies

Data Availability

No additional data are available.

Conflicts of Interest

The authors declare no conflict of interest.

Acknowledgments

This work was supported by the National Natural Science Foundation of China (No. 42172172 and No. 41802123).

References

[1] A. L. Jia, Z. Guo, J. L. Guo, and H. J. Yan, "Research achievements on reservoir geological modeling of China in the past three decades," *Acta Petrolei Sinica*, vol. 42, no. 11, pp. 1506–1515, 2021.

[2] X. X. Li, *Construction and application of fluvial fan deposition database*, China University of Geosciences (Beijing), 2021.

[3] W. B. Zhang, Z. Q. Liu, Z. H. Chen, H. M. Xu, Y. Lin, and J. W. Wang, "Establishment and application of geological data base on deep-water channels in Angola block," *Acta Sedimentologica Sinica*, vol. 33, no. 1, pp. 142–152, 2015.

[4] L. Colombera, N. P. Mountney, C. E. Russell, M. N. Shiers, and W. D. Mccaffrey, "Geometry and compartmentalization of fluvial meander-belt reservoirs at the bar-form scale: Quantitative insight from outcrop, modern and subsurface analogues," *Marine and Petroleum Geology*, vol. 82, pp. 35–55, 2017.

[5] Z. B. Xu, C. S. Shen, Y. K. Chen et al., "Architecture characterization for sandy braided river reservoir and controlling factors of remaining oil distribution——a case study of P oilfield (Neogene), Bohai offshore, China," *Acta Sedimentologica Sinica*, vol. 34, no. 2, pp. 375–385, 2016.

[6] S. H. Li, C. M. Zhang, K. X. Lin, T. J. Yin, and C. S. Zhang, "The construction of prototype models in reservoir modeling," *Sedimentary Geology and Tethyan Geology*, vol. 24, no. 3, pp. 102–107, 2004.

[7] S. Y. Shi, S. Y. Hu, W. J. Feng, and W. Liu, "Buliding geological knowledge database based on Google Earth software," *Acta Sedimentologica Sinica*, vol. 30, no. 5, pp. 869–878, 2012.

[8] J. Zhang, K. F. Hou, F. P. Li, M. Tian, and Z. G. Zhang, "Reserves evaluation of tight sandstone gas reservoir based on reservoir geological knowledge database: a case study of Su14 block in Sulige Gasfield, Ordos Basin," *Natural Gas Geoscience*, vol. 28, no. 9, pp. 1322–1329, 2017.

[9] T. B. Yang, J. P. Wang, Y. Wang, B. F. W. Xue, and Q. Hao, "Reservoir modeling of tight sandstone gas reservoir based on geological knowledge database: a case from Su X block in Sulige Gas Field," *Lithologic Reservoirs*, vol. 29, no. 4, pp. 138–145, 2017.

[10] S. H. Li, R. M. Han, C. M. Zhang, B. Q. Zhang, T. Hu, and Z. G. Shu, "Integration of outcrop in reservoir modeling," *Natural Gas Geoscience*, vol. 17, no. 3, pp. 374–377, 2006.

[11] S. Kelly, *Scaling and Hierarchy in Braided Rivers and their Deposits: Examples and Implications for Reservoir Modelling*, Blackwell Publishing Ltd, 2009.

[12] M. Ghinassi, W. Nemec, M. Aldinucci, S. Nehyba, V. Ozaksoy, and F. Fidolini, "Plan-form evolution of ancient meandering rivers reconstructed from longitudinal outcrop sections," *Sedimentology*, vol. 61, no. 4, pp. 952–977, 2014.

[13] B. J. Willis and H. Tang, "Three-dimensional connectivity of point-bar deposits," *Journal of Sedimentary Research*, vol. 80, no. 5, pp. 440–454, 2010.

[14] Y. Y. Li, *The Braided River Flume Simulation Experiment and the Design of Reservoir Geological Knowledge Base*, Yangtze University, 2018.

[15] S. L. Yin, Y. Gao, Z. M. Hu et al., "Multiple-point geostatistical simulation of outcrop based on UAV oblique photographic data: a case study of Shihezi Formation in Pingtou township, Lvliang city, Shanxi," *Acta Petrolei Sinica*, vol. 42, no. 2, pp. 198–216, 2021.

[16] A. Pickel, J. D. Frechette, A. Comunian, and G. S. Weissmann, "Building a training image with Digital Outcrop Models," *Journal of Hydrology*, vol. 531, pp. 53–61, 2015.

[17] S. M. Hudson, S. Meek, B. J. Steeves et al., "Characterization of complex fluvial architecture through outcrop studies—dealing with intrinsic data bias at multiple scales in the pursuit of a representative geomodel," *Bulletin of Canadian Petroleum Geology*, vol. 67, no. 4, pp. 231–254, 2019.

[18] X. F. Qin, R. Qi, W. Li, and X. M. Chen, "Braided channel architecture analysis and semi-quantitative seismic prediction for channel bars in P1x1 of the Hangjinqi area, Ordos basin, China," *Geophysical Prospecting for Petroleum*, vol. 58, no. 4, pp. 572–579, 2019.

[19] D. Q. Xu, Z. X. Sun, Y. F. Ren, and C. Yang, "Geological modeling of braided river tight reservoir based on geological knowledge database," *Fault-Block Oil & Gas Field*, vol. 25, no. 1, pp. 57–61, 2018.

[20] S. Z. Shen, C. Y. Lin, L. H. Ren, W. J. Liu, H. P. Chen, and W. S. Huang, "Establishment of the depositional model of sandy braided river: a case from the H block in Orinoco Heavy Oil Belt, Venezuela," *Acta Sedimentologica Sinica*, vol. 33, no. 5, pp. 965–971, 2015.

[21] X. H. Zhang, C. M. Zhang, W. J. Feng et al., "Geometry and control factors of distributive fluvial system around the Sugan Lake basin," *Acta Geologica Sinica*, vol. 93, no. 11, pp. 2947–2959, 2019.

[22] Z. F. Yi, S. F. Zhang, Y. N. Wang, E. Z. Xu, S. H. Zhao, and Y. Y. Wang, "Quantitative characterization of point bar sand bodies in meandering river under different curvatures: a case study of modern deposition of Baihe river in the source area of Yellow River," *Lithologic Reservoirs*, vol. 34, no. 1, pp. 34–42, 2022.

[23] G. Q. Zhang, X. Y. Hu, C. Jia, B. Liu, and J. D. Liu, "Construction of a quantitative geological knowledge base for the braided river of Hanggin Banner and its application," *Journal of Southwest Petroleum University (Science & Technology Edition)*, vol. 40, no. 4, pp. 79–89, 2018.

[24] A. L. Jia, J. W. Tang, D. B. He, Y. C. Ji, and L. H. Cheng, "Geological modeling for sandstone reservoirs with low permeability and strong heterogeneity in Sulige Gasfield," *China Petroleum Exploration*, vol. 12, no. 1, pp. 12–16, 2007.

[25] H. Y. Li, Y. Gao, Y. J. Wang, X. G. Sun, Z. Yang, and R. Zhao, "Intercalation pattern and its impact on development of braided river reservoirs: a case of Fengcheng Oilfield, Junggar Basin, NW China," *Petroleum Exploration and Development*, vol. 42, no. 3, pp. 397–407, 2015.

[26] Z. X. Ma, Z. Wu, J. Zhang et al., "Static and dynamic information fusion based reservoir architecture characterization and 3D geological modeling technology for braided river reservoirs," *Natural Gas Industry*, vol. 42, no. 1, pp. 146–158, 2022.

[27] S. Z. Chen, C. Y. Lin, L. H. Ren, X. G. Zhang, and W. S. Huang, "Geological modeling of braided river reservoir constrained by genetic and evolutionary information: a case study of block m in Orinoco heavy oil belt, Venezuela," *Oil Geophysical Prospecting*, vol. 55, no. 5, pp. 1092–1101, 2020.

[28] X. J. Wu, H. B. Su, S. J. Zhang, L. J. Feng, J. Wang, and S. L. Yin, "Architecture anatomy and hierarchical modeling of sand-gravel braided river reservoirs: a case study of Zhong32 wells area, Qigu Formation reservoir, Fengceng oilfield," *Acta Sedimentologica Sinica*, vol. 38, no. 5, pp. 933–945, 2020.

[29] C. Y. Liu, H. G. Zhao, X. J. Gui, L. P. Yue, J. F. Zhao, and J. Q. Wang, "Space-time coordinate of the evolution and reformation and mineralization response in Ordos Basin," *Acta Geologica Sinica*, vol. 80, no. 5, pp. 617–638, 2006.

[30] J. H. Fu, X. S. Wei, and J. F. Ren, "Distribution and genesis of large-scale Upper Paleozoic lithologic gas reservoirs on Yi-Shaan Slope," *Petroleum Exploration and Development*, vol. 35, no. 6, pp. 664–691, 2008.

[31] J. J. Wu, *Gas Reservoir Evaluation of Tight Sandstone in He-1 Member of Daniudi Gas Field in Ordos Basin*, Chengdu University of Technology, 2013.

[32] D. Y. Chen, *Characterization of braided river reservoir architecture in Northeastern Ordos Basin—based on the study of He 8 member on Fugu Tianshengqiao outcrop*, Chengdu University of Technology, 2019.

[33] Q. H. Xu, W. Z. Shi, X. Y. Xie et al., "Multichannel systems in an ancient river-dominated delta: case study of the lower Yanchang Formation, southwest Ordos Basin, China," *Canadian Journal of Earth Sciences*, vol. 56, no. 10, pp. 1027–1040, 2019.

[34] N. N. Xu, S. P. Zhang, Y. S. Wang, and L. W. Qiu, "Diagenesis and pore formation of the upper Paleozoic tight sandstone in the northern area of the Ordos Basin," *Acta Sedimentologica Sinica*, vol. 40, no. 2, pp. 422–434, 2022.

[35] Y. H. Xu and D. F. He, "Triassic provenance shifts and tectonic evolution of southeast Ordos Basin, Central China," *Palaeogeography, Palaeoclimatology, Palaeoecology*, vol. 598, article 111002, 2022.

[36] J. A. Howell, A. W. Martinius, and T. R. Good, "The application of outcrop analogues in geological modelling: a review, present status and future outlook," *Geological Society of London*, vol. 387, no. 1, pp. 1–25, 2014.

[37] J. S. Bridge and R. S. Tye, "Interpreting the dimensions of ancient fluvial channel bars, channels, and channel belts from wireline-logs and cores," *AAPG Bulletin*, vol. 84, no. 8, pp. 1205–1228, 2000.

[38] W. L. He, S. H. Li, J. Wang, Y. G. Zhang, J. B. Yu, and J. H. Shi, "Characteristics and key controlling factors of channel bar in different types of braided river based on sink simulation experiments," *Journal of Northeast Petroleum University*, vol. 43, no. 6, pp. 13–22, 2019.

[39] W. Wang, *Study of the slope fan within the delta front using sedimentary simulation experiment*, China University of Petroleum (East China), 2018.

[40] Y. Tang, T. J. Yin, J. H. Qing, and D. D. Wang, "Development of large-scale shallow-water fan delta: sedimentary laboratory simulation and experiments," *Xinjiang Petroleum Geology*, vol. 38, no. 3, pp. 253–263, 2017.

[41] Y. J. Zhu, R. Xia, Y. K. Zheng et al., "Architectures and evolution of arid alluvial fans: insights from a flume experiment," *Journal of Palaeogeography*, vol. 22, no. 6, pp. 1081–1094, 2020.

[42] M. J. Pyrcz, R. P. Sech, J. A. Covault et al., "Stratigraphic rule-based reservoir modeling," *Bulletin of Canadian Petroleum Geology*, vol. 63, no. 4, pp. 287–303, 2015.

[43] M. C. Wang, X. F. Shang, and T. Z. Duan, "A review of the establishment methods of training image in multiple-point statistics modeling," *Geological Journal of China Universities*, vol. 28, no. 1, pp. 96–103, 2022.